JGR Oceans

RESEARCH ARTICLE
10.1029/2023JC020354

Integrating Climatological-Hydrodynamic Modeling and Paleohurricane Records to Assess Storm Surge Risk

Amirhosein Begmohammadi[1], Christine Y. Blackshaw[1], Ning Lin[1], Avantika Gori[1], Elizabeth Wallace[2], Kerry Emanuel[3], and Jeffrey P. Donnelly[4]

[1]Department of Civil and Environmental Engineering, Princeton University, Princeton, NJ, USA, [2]Department of Earth and Ocean Sciences, Old Dominion University, Norfolk, VA, USA, [3]Lorenz Center, Massachusetts Institute of Technology, Cambridge, MA, USA, [4]Department of Geology and Geophysics, Woods Hole Oceanographic Institution, Woods Hole, MA, USA

Key Points:

- Hydrodynamic modeling is used to identify event beds in paleorecords
- Storm sizes and surges at the sediment site are reconstructed for 1850–2016 to bias-correct climatological-hydrodynamic modeling results
- The surge risk under two carbon emission scenarios (SSP2-4.5, SSP5-8.5) and sea level rise is quantified for Long Island, Bahamas

Correspondence to:

A. Begmohammadi,
begmohammadi@princeton.edu

Citation:

Begmohammadi, A., Blackshaw, C. Y., Lin, N., Gori, A., Wallace, E., Emanuel, K., & Donnelly, J. P. (2024). Integrating climatological-hydrodynamic modeling and paleohurricane records to assess Storm surge risk. *Journal of Geophysical Research: Oceans*, *129*, e2023JC020354. https://doi.org/10.1029/2023JC020354

Received 10 AUG 2023
Accepted 28 DEC 2023

Author Contributions:

Conceptualization: Amirhosein Begmohammadi, Christine Y. Blackshaw, Ning Lin, Avantika Gori
Data curation: Elizabeth Wallace
Formal analysis: Amirhosein Begmohammadi, Christine Y. Blackshaw, Avantika Gori, Elizabeth Wallace
Methodology: Amirhosein Begmohammadi, Christine Y. Blackshaw, Ning Lin, Avantika Gori, Kerry Emanuel
Supervision: Ning Lin
Validation: Amirhosein Begmohammadi, Christine Y. Blackshaw
Writing – original draft: Amirhosein Begmohammadi, Christine Y. Blackshaw
Writing – review & editing: Amirhosein Begmohammadi, Ning Lin, Elizabeth Wallace, Kerry Emanuel, Jeffrey P. Donnelly

Abstract Sediment cores from blue holes have emerged as a promising tool for extending the record of long-term tropical cyclone (TC) activity. However, interpreting this archive is challenging because storm surge depends on many parameters including TC intensity, track, and size. In this study, we use climatological-hydrodynamic modeling to interpret paleohurricane sediment records between 1851 and 2016 and assess the storm surge risk for Long Island in The Bahamas. As the historical TC data from 1988 to 2016 is too limited to estimate the surge risk for this area, we use historical event attribution in paleorecords paired with synthetic storm modeling to estimate TC parameters that are often lacking in earlier historical records (i.e., the radius of maximum wind for storms before 1988). We then reconstruct storm surges at the sediment site for a longer time period of 1851–2016 (the extent of hurricane Best Track records). The reconstructed surges are used to verify and bias-correct the climatological-hydrodynamic modeling results. The analysis reveals a significant risk for Long Island in The Bahamas, with an estimated 500-year stormtide of around 1.63 ± 0.26 m, slightly exceeding the largest recorded level at site between 1988 and 2015. Finally, we apply the bias-corrected climatological-hydrodynamic modeling to quantify the surge risk under two carbon emission scenarios. Due to sea level rise and TC climatology change, the 500-year stormtide would become 2.69 ± 0.50 and 3.29 ± 0.82 m for SSP2-4.5 and SSP5-8.5, respectively by the end of the 21st century.

Plain Language Summary Paleohurricane sediment records can capture tropical cyclone (TC) landfall and associated storm surge severity over several millennia, providing an extended record to quantify long-term storm surge risk. Interpretation of these records is difficult because storm surge depends on many parameters such as TC intensity, track, and size. In this study, we use hydrodynamic modeling to identify which historical TCs between 1851 and 2016 transported sediment into underwater sinkholes near Long Island in The Bahamas. Supplementing the historical record with synthetic TCs created by a computer model, we leverage our interpretation of the paleorecord to approximate the size and surge level for storms prior to 1988 for which observations are unavailable. Next, we integrate the reconstructed storm surge levels and climatological-hydrodynamic modeling to estimate long-term storm surge hazards for the area. Finally, we apply the integrated model to assess storm surge risk for Long Island under future climates (SSP2-4.5 and SSP5-8.5) and sea level rise and find a significant increase in TC hazard risk for this location by the end of the century.

1. Introduction

Storm surge from tropical cyclones (TCs), also called hurricanes, is one of the most devastating coastal hazards, causing millions of dollars in damage and the majority of TC related deaths (Davlasheridze et al., 2019). The compounding effects of growing coastal populations, changing TC climatology from warmer oceans, and sea-level-rise (SLR) contribute to the increased vulnerability of coastal communities to more intense storm surge events (K. A. Emanuel, 2013; Knutson et al., 2020; Lin et al., 2012; Woodruff et al., 2013). Developing effective solutions to mitigate TC surge disasters requires understanding the risk of TC surge inundation. Historical TC and storm surge records are often too limited, however, to quantify current and future TC risk to local populations. Prior to the development of reliable satellite tracking in the 1960s, we rely on early aircraft and ship log observations over the ocean for historical TCs that only date back to the year 1851. In addition, these early observations do not have information on critical storm characteristics, especially storm size, characterized by

radius of maximum wind (R_{max}) (Knapp et al., 2010). Although recent work has reconstructed storm size for many historical TCs, these reconstructions only date back to 1950 (Gori et al., 2023). The short observational records of hurricane activity make it difficult to evaluate TC behavior over long time scales and to make accurate future projections.

A well practiced approach to modeling TC surge risk is through climatological-hydrodynamic modeling. Most TC risk models augment the historical TC records by generating synthetic TCs based on historical observed climatology (Scheffner et al., 1996; Toro et al., 2010; Vickery et al., 2000). However, those methods may produce storms that are not physically realistic and because they rely on historical data, they cannot capture changes in TC climatology induced by climate change. Another approach is to utilize a statistical-deterministic TC risk model that is environment-dependent (K. Emanuel et al., 2006). In this method, vortices are randomly seeded over the ocean and moved according to the statistics of the environmental wind. The characteristics of synthetic storms are modeled deterministically given the atmosphere and oceanic conditions along the storm track. This approach generates a very large number of synthetic storms throughout an ocean basin to obtain a representative sample of time-varying realistic storms affecting the location of interest. This TC risk model has been combined with hydrodynamic models to evaluate local surge risk (Gori et al., 2022; Lin et al., 2012; Marsooli et al., 2019).

The field of paleotempestology has emerged as a new tool for reconstructing long-term TC activity (Brandon et al., 2013; Donnelly & Woodruff, 2007; Liu & Fearn, 1993, 2000; Tan et al., 2023; Tao et al., 2021; van Hengstum et al., 2014; Yang et al., 2020, 2022). Paleotempestological records identify and date signatures of storm landfalls in natural archives (e.g., coarse grains in sediment cores (Donnelly & Woodruff, 2007; Liu & Fearn, 1993), increased latewood width in tree cores (Maxwell et al., 2021)). These archives then provide a record of TC occurrence in a given area that extends back hundreds to thousands of years. Most paleohurricane proxies are sourced from sediment based archives that capture coarse grained sediments that are mobilized and then deposited in coastal basins by high energy waves associated with TCs. McKee and Blumenstock were among the pioneers who recognized the potential of using overwash deposits to reconstruct TC events (Blumenstock, 1958; McKee, 1959). Over time, researchers have built an extensive network of paleohurricane archives across various environments (E. J. Wallace, Dee, & Emanuel, 2021), including lakes (Liu & Fearn, 2000), coastal wetlands (Boldt et al., 2010; Donnelly et al., 2001; McCloskey & Keller, 2009), and back-barrier lagoons (Davis et al., 1989; Donnelly & Woodruff, 2007). Recent work has expanded paleohurricane research into the hurricane-prone tropical Atlantic using sediment records collected from coastal karst basins, including fully submerged blue holes (Schmitt et al., 2020; E. Wallace et al., 2019; Winkler et al., 2020) and sub-aerial sinkholes (Brandon et al., 2013; Brown et al., 2014; Lane et al., 2011). CKBs are basin-like features found in tropical locations worldwide that originate from dissolution processes on carbonate platforms (Maloney & Hartmann, 2000; van Hengstum et al., 2014). These basins are well suited for producing paleoTC archives because (a) they have large accommodation spaces that allow sediment accumulation (Dill, 1970), (b) they have anoxic conditions at the bottom which limit bioturbation (Gischler et al., 2008), and (c) they are often surrounded by reefs and tidal flats which provide abundant sediment supply (Gischler et al., 2008; Shinn et al., 1996). In particular, paleohurricane records from blue holes (Schmitt et al., 2020; E. Wallace et al., 2021; Winkler et al., 2020) are typically very high resolution (annual to near annual) which allows these archives to resolve many different storms from the observational records unlike other low resolution archives (McCloskey & Keller, 2009).

It is challenging to interpret these long-term paleohurricane records due to age uncertainties in the sediment cores, and limited information about past climate conditions and morphology of the coastline. Despite uncertainties, paleohurricane records still provide useful information for long term TC risk assessment. For instance, Lin et al. (2014) used both climatological-hydrodynamic modeling and paleorecords to address TC surge risk for northwest Florida. They found that both the synthetic database and paleorecords contain a much higher frequency of extreme events than the historical record at Apalachee Bay, FL. In this study, we extend this framework to further integrate paleorecords and climatological-hydrodynamic modeling to estimate storm surge risk for Long Island blue hole (LIBH) in The Bahamas.

In the spring of 2016, E. Wallace et al. (2021) collected sediment cores from a blue hole on Long Island in The Bahamas. The authors identified coarse grained event beds preserved in their cores resulting from TC strikes on the island and evaluated the frequency of TC activity over the past 1,050 years. Although paleorecords allow us to reconstruct the overall frequency of TCs over hundreds or thousands of years, determining the essential storm characteristics of past events from sedimentary deposits can be more challenging as storm surge depends on

various parameters, including the track and intensity of the TCs, the site configuration, etc. In addition, age uncertainties in the sediment cores and a lack of observations during storm events make it difficult to exactly pinpoint which storm events contributed to the coarse layers. Here, to strengthen paleohurricane interpretations, we use hydrodynamic and synthetic TC modeling to identify storms that could produce coarse anomalies in the Long Island paleohurricane record and reconstruct unknown characteristics of historical storms based on the sediment data. Then, we employ the approach of combining climatological-hydrodynamic modeling with reconstructed records to estimate surge risk on Long Island. Finally, we apply the combined modeling to quantify the effects of sea level rise (SLR) and TC climatology change (under two carbon emission scenarios SSP2-4.5 and SSP5-8.5) on late 21st century surge hazards on Long Island in The Bahamas.

2. Method

2.1. Study Site

Long Island is located on the eastern margin of the Great Bahama Bank and is split by the Tropic of Cancer. The blue hole (LIBH), 150 m in diameter and 12 m deep, is located 400 m off the northwest shore of Long Island (N 23.265°, W 75.117°) (E. Wallace et al., 2021) (see Figure 1a). Under ambient conditions, fine-grained sediment produced on the surrounding carbonate platform accumulates in the blue hole at a rate of about 1 cm/yr. During storm events, on the other hand, coarse grained sediment is transported and deposited into the basin. The near annual resolution of the sediment record from LIBH allows for distinguishing sediment layers created by storm events that occur within 1–2 years of each other (see Figure 1b).

Since 1851, 34 TCs have passed within 100 km of LIBH. Four major hurricanes (above category 2) passed by Long Island since 2010: Matthew 2016, Joaquin 2015, Sandy 2012, and Irene 2011. The close passage of these intense hurricanes caused major damage to the island. For example, in 2015, the center of circulation of Hurricane Joaquin passed 40 km east of LIBH at Category 4 strength. Power lines were downed, private fresh water wells were flooded, and structural damage occurred to homes; approximately 49% of the 413 Bahamian residences destroyed were located in Long Island (Virgil, N.D.). Over two-thirds of the island remained inundated with 1.2–1.8 m of water for almost a week after impact, blocking coastal roads and damaging the marina (Robbie, 2016). The impact of a single storm like Joaquin could be amplified by changing TC climatology and SLR. Long Island itself does not have any active tidal gauges. In fact, the only tidal gauge in the entire Bahamas Archipelago is located on the most northwestern point of the Grand Bahamas island. The lack of current data collection for the Bahamas area emphasizes the importance of using paleorecords along with TC risk modeling for this region.

Coarse-grained deposits in the Long Island paleohurricane archive show that the island has experienced frequent storm strikes over the last 1,000 years (E. Wallace et al., 2021) (see Figure 1b). Event beds in the LIBH paleohurricane record were identified by applying a cutoff threshold to the coarse anomaly data (Donnelly et al., 2015; E. Wallace et al., 2019). All peaks in coarse anomaly above 5.9% are considered storm event beds. The ages of these event beds are estimated using a Bayesian age model (Blaauw & Christen, 2011) combining lead-210 dates, pollen evidence of land use activities and radiocarbon dates from terrestrial macrofossils (E. Wallace et al., 2021).

Here, we consider the modern period between 1851 and 2016, when the Best Track information (Knapp et al., 2010) of TCs is available. Figure 1b demonstrates that E. Wallace et al. (2021) identified seven event beds in the LIBH record whose estimated dates fall between 1851 and 2016. Previously, the authors used the Sea, Lake and Overland Surges from Hurricanes (SLOSH) (Jelesnianski, 1992) storm surge model to identify the storm events that left deposits at LIBH. However, the SLOSH model does not consider the tidal flow, only adjusting the maximum high tide to the initial mean sea level, and also uses a relatively coarse grid (5×5 km^2), which reduces the accuracy of the model. According to the results from the SLOSH model, the authors could identify a few potential hurricanes for each event bed. Here, we utilize the ADvanced CIRCulation (ADCIRC) model (Luettich et al., 1992) to more confidently match each event beds to a specific historical TC, taking into account tidal effects and operating the simulation on a high-resolution mesh to achieve higher accuracy surge results for Long Island.

The Long Island site is chosen in this study as it captured a large number of modern event beds and most of those event beds were well dated with pollen, post-bomb radiocarbon, and lead-210 chronological tie-points (E. Wallace et al., 2021). We are only able to validate our ADCIRC experiments using TCs in the time frame of 1988–2016, so Long Island was the most suitable choice for our analysis given its high frequency of well dated modern event beds compared to other records (in neighbor islands including South Andros, Middle Caicos, Abaco, Grand Bahama, and Cay Sal). In addition, LIBH (E. Wallace et al., 2021) is well suited for hydrodynamic

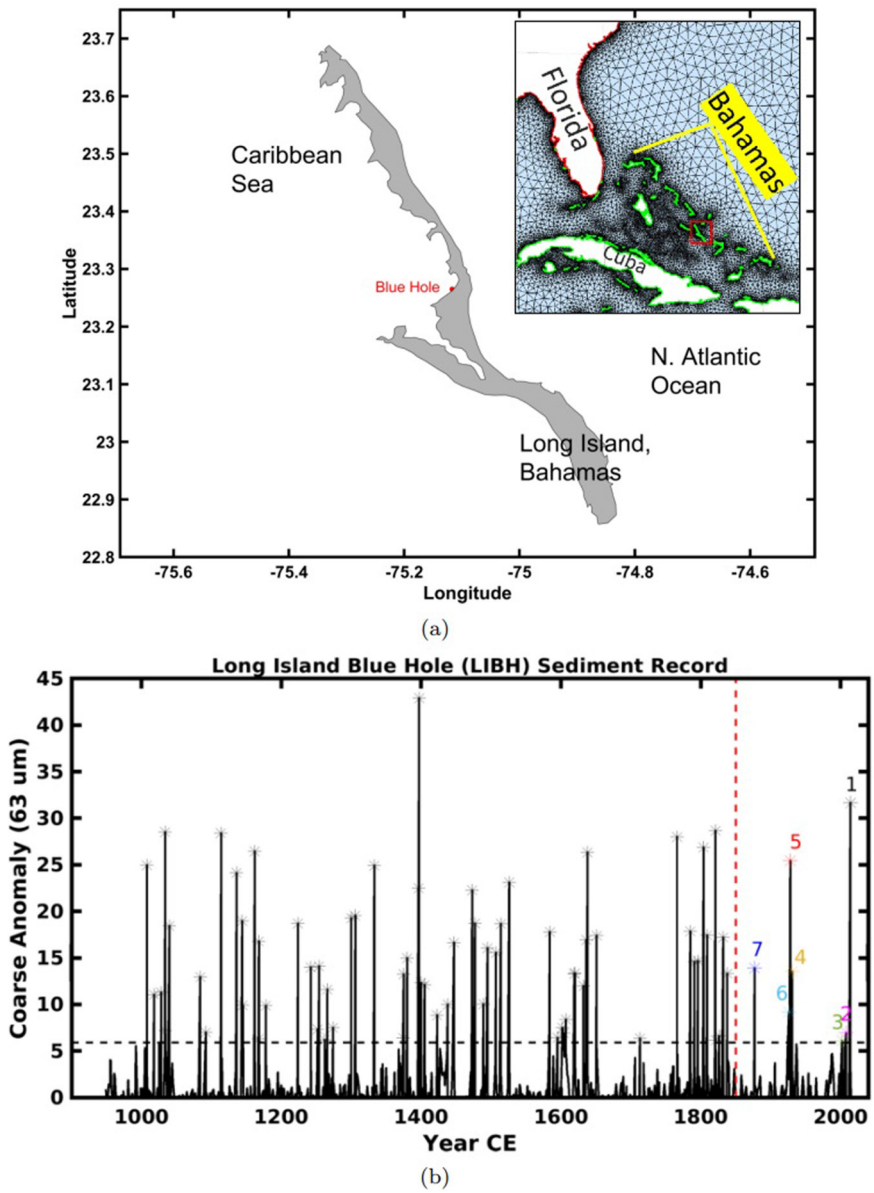

Figure 1. (a) Map of Long Island, The Bahamas. The larger area shows the unstructured triangular mesh for ADvanced CIRCulation. (b) Coarse anomaly plot (solid line) for Long Island blue hole as a function of time (E. Wallace et al., 2021). The dashed black line is the event bed threshold of 5.90%. The dashed red line denotes the year of 1850.

experiments because the geomorphology of the surrounding carbonate platform is relatively simple compared to the other blue hole sites (E. Wallace et al., 2019; E. J. Wallace, Donnelly, et al., 2021; Winkler et al., 2020). Many other blue hole records from the neighbor islands are nestled in complex tidal flats (Andros Island (E. Wallace et al., 2019), Abaco Island (E. Wallace et al., 2021)) or surrounded by sub-aerial shoals (Caicos Island (E. J. Wallace, Donnelly, et al., 2021)) that are difficult to model without detailed topographic or bathymetric data. In this paper, we aim to explore the application of hydrodynamic modeling for paloehurricane reconstruction; the application to the simple blue hole environments may be scaled up to more complex sites in future work.

2.2. Hydrodynamic Modeling

Among numerical storm surge models (Begmohammadi et al., 2022; Jelesnianski, 1992; Kennedy et al., 2019; Luettich et al., 1992; Roelvink & Van Banning, 1995), ADCIRC is a widely used storm surge model that uses a

finite element method over unstructured triangular meshes (Luettich et al., 1992). A single mesh can have varying resolution throughout its representation of a physical area: up to several kilometers in the open ocean, down to meters in small-scale inland areas. ADCIRC describes the physical processes associated with the storm surge, and can incorporate the effects of astronomical tide. It also can consider the effects of wind waves when coupled with the wave model SWAN (Dietrich et al., 2011). The model has been validated for storm surge along the U.S. Gulf and Atlantic coasts (Deb & Ferreira, 2018; Dietrich et al., 2011; Hope et al., 2013; Lin, Smith, et al., 2010; Marsooli & Lin, 2018). However, ADCIRC simulations can be computationally expensive, and it is not feasible to apply ADCIRC for very large numbers of simulations on high-resolution (down to 100 m element size) meshes. As a result, relatively coarse meshes ($O \simeq 1$ km at the coastlines (Marsooli & Lin, 2018)) are often used to describe coastal features.

To model storms that pass Long Island, we built two ADCIRC meshes (fine and coarse resolution) with OceanMesh2D (Roberts et al., 2019) to cover the Gulf of Mexico and the Atlantic Ocean. The higher resolution mesh includes 376,814 elements and 221,706 nodes. The minimum resolution of elements is around 0.5 km near the coastlines. The coarser mesh consists of 95,920 elements and 54,916 nodes with a minimum resolution of 2 km along the coastlines. The bathymetric data were obtained from global bathymetry and topography at one arc sec (SRTM15+) (Tozer et al., 2019), which is approximately 0.5 km resolution. All of the historical events are run on the high resolution mesh, while the synthetic storms are run on the coarse resolution mesh. Note that these meshes are superior to the SLOSH model used by the previous study for this area (E. Wallace et al., 2021) in terms of accuracy.

To account for tide, eight tidal constituents enforce ocean boundaries of the mesh to consider the tidal effects in the model. Tidal data are obtained from the global model of ocean tides, TPXO8-ATLAS (Egbert & Erofeeva, 2002). The timing of the tide is matched with the timing of the observations (Hope et al., 2013; Pringle et al., 2021).

2.3. Event Attribution and Reconstruction

We can develop a first order understanding of how Long Island sediment proxies respond to various storm events by pinpointing the modern storms (from 1850 CE to the present) that have deposited coarse materials in the Blue Hole. To do so, we assume that higher surges during hurricane events mobilize and resuspend coarse grained benthic sediment on the shallow carbonate platform surrounding the blue hole. Some of that sediment moves into the blue hole which acts as a natural settling tube (Winkler et al., 2020). The process of sediment transport during storm surges is highly complex, influenced by factors such as sediment grain sizes and local bathymetry. Modeling this phenomenon is exceptionally challenging, requiring high-resolution bathymetric data, detailed maps of surface sediments, 3-D hydrodynamic models, and the coupling of sediment transport models with hydrodynamic models, among other factors. These modeling efforts are computationally expensive. Additionally, we are constrained by the lack of high-resolution bathymetric data in this area and limited information about bed grain sediment sizes and densities. We also lack information about how the bathymetry of this area has changed over time. Due to these constraints, we are unable to establish a relationship between coarse anomalies and surge height. However, if we can identify the lowest surge within the time frame 1988–2016 (when all storm track information is available) that caused sediment deposition, and we proceed by assuming that surges above this specific threshold can also result in deposition at LIBH.

Specifically, to interpret the record of modern storms, we match historical TCs that pass LIBH to the event beds in the record. We use the North Atlantic Best Track data set (referred to as best Track) (Knapp et al., 2010) for historical records of TC properties. We consider two time windows for our analysis based on availability of TC records in the Best Track database. The first window spans from 1988 to 2016 within which TC information for the track, minimum pressure of the hurricane center, radius of maximum wind, and maximum wind speed are all available. This information enables us to develop a surge threshold for potential TCs to leave a deposit at LIBH, in order to attribute the seven event beds to specific historical TC.

For the second time window between 1851 and 1987, radius of maximum wind and minimum pressure of the hurricane center observations are unavailable (minimum pressure is available from 1950). To obtain a first estimation of the surge level, we use a method based on empirical relationships of hurricane characteristics to estimate the radius of maximum wind and minimum central pressure of hurricanes. To approximate the central pressure of hurricanes, we apply a simple wind-pressure relationship based on the cyclostrophic balance equation

presented by Knaff and Zehr (Knaff & Zehr, 2007). Then, to estimate the radius of maximum wind, we adopt an empirical formula proposed by the U.S. Federal Emergency Management Agency ((FEMA), 2012), which is a function of the minimum central pressure of hurricanes and latitude. We account for uncertainty in the estimates for radius of maximum wind and minimum central pressure by varying the minimum central pressure value by ±15 mb and then updating the estimation of radius of maximum wind. This pressure range is derived from the 95% quantile of the differences between actual central pressure and calculated central pressure from the empirical formula for TCs between 1988 and 2016.

Having attributed the event beds from 1851 to 2016, we can develop more accurate estimations for radius of maximum wind and surge levels for deposit-leaving TCs. Given the presence of a historical TC in the paleorecord, we can use the shared properties of the synthetic (see next Section 2.4) and historic TCs to estimate unknown storm characteristics, in particular storm size (R_{max}). For example, historic TCs that passed LIBH prior to 1988 do not have observed R_{max} values. We can group these pre-1988 historical storms with synthetic and post 1988 historical TCs based on observed properties that are available including intensity and storm track (position and direction) to estimate R_{max} values for pre-1988 historical storms. We use the K-means clusters (Duda et al., 1973) to identify R_{max} from the storm properties for deposit-leaving TCs. K-means clustering is a numerical, unsupervised, non-deterministic, iterative method that is both computationally efficient and easy to implement in many practical applications (Babatunde et al., 2019; Carvalho et al., 2016). Finally, we use the information obtained from this process to estimate the surge level associated with each historical event.

2.4. Synthetic Storms

We used a statistical-deterministic TC model (K. Emanuel et al., 2006) to generate a large number of synthetic TCs. The synthetic storms are generated using gridded atmosphere and ocean data products, including General Circulation Models (GCMs) or reanalysis data. Storms are produced in a three step process. First, warm core vortices are placed randomly in space and time. Vortices that meet favorable environmental conditions develop into TCs. Next, each genesis point is given a track according to the daily large-scale environmental winds in the model plus a beta-drift correction (Holland, 1982). Finally, at each time step, TC intensity is predicted based on the Coupled Hurricane Intensity Prediction System, which is an axisymmetric vortex model coupled to a 1D ocean model (K. Emanuel et al., 2004). To represent historical TC climatology from 1988 to 2016, synthetic tracks were generated based on the National Center for Environmental Prediction (NCEP) reanalysis product (Kalnay et al., 1996). To represent TC climatology under future possible climate (2070–2100) conditions, two emission scenarios from the Shared Socioeconomic Pathways were considered—a moderate (SSP2 4.5) and high (SSP5 8.5) scenario. For each future scenario, the synthetic tracks were generated based on each of six CMIP6 climate models: Canadian Earth System Model, Centre National de Recherches Météorologiques (CNRM), EC-Earth Consortium Model (ECEARTH), The Institute Pierre Simon Laplace Climate Model (IPSL), Model for Interdisciplinary Research on Climate, and United Kingdom Meteorological Office.

All synthetic storms are run on ADCIRC coarse resolution mesh for 7 days. The model accounts for tides through the use of open ocean boundary conditions as well as wind and pressure fields, which are developed based on physics-based parametric models. The parametric models take into account the TCs' maximum wind speed V_{max} and radius of maximum wind R_{max} (K. Emanuel & Rotunno, 2011; Holland, 1980) to produce the spatial and temporal wind and pressure fields. To account for the asymmetry of the wind field, an empirically estimated surface background wind vector by Lin and Chavas (2012) is used.

The generated future TCs from each climate model are likely biased in their intensity and annual frequency compared to the NCEP TCs. Consequently, the biases in TCs can lead to biases in hazard estimation, as intensity and frequency are dominant drivers impacting coastal storm surge risk. Here, we perform bias correction for TC intensity and annual frequency at the storm level.

First, the quantile delta mapping approach (Cannon et al., 2015) is used in order to correct the GCM projected TC intensity (V_{Max}) of each TC set. The change between the GCM-projected future (2070–2100) and historical (1988–2015) downscaled V_{Max} quantiles is added to the NCEP downscaled historical quantiles to create a corrected future V_{Max} distribution for each GCM model. Using the ratio of the corrected V_{Max} probability density to the GCM projected V_{Max} probability density, the GCM projected storms are weighted and re-sampled (Tokdar & Kass, 2010). By doing so, we are able to match the corrected future V_{Max} distribution and consequently generate

a new TC set. Second, the bias correction of TC frequency is performed by calculating the ratio of the GCM future frequency to the GCM historical frequency and multiplying the ratio by the NCEP historical frequency GCM-predicted frequency change to the NCEP-derived frequency (for more details on bias correction see Gori et al. (2022)).

We select TCs within a radius of 100 km of LIBH because previous work (E. Wallace et al., 2021) suggests that the LIBH sediment record is only sensitive to storms passing within this radius (see Section 3). Overall, there are 1244 TCs in the historical time period (NCEP), 3,745 TCs for SSP2-4.5, and 3,848 TCs for SSP5-8.5. We perform ADCIRC simulation for all selected storms in the historical period. To reduce the computational cost, we sampled 1,200 TCs for each climate scenario so that the sample storms have the same intensity distribution as the original data set. The synthetic storms correspond to 1,220 simulation years in the historical climate and the sampled future storms correspond to 692 (408) simulation years under the SSP2-4.5 (SSP5-8.5) scenario.

After reconstructing the historical hurricanes between 1851 and 2016, we apply bias correction to the estimated surge return levels using the reconstructions from 1851 to 2016 to account for possible biases in the TC and hydrodynamic models. We bias correct the frequency by computing the ratio of the NCEP frequency to the observed historical frequency and multiplying it by the GCM future frequency. For the historical period, the NCEP frequency is simply adjusted to equal the historical observed frequency. We then bias correct the probability distribution of peak storm surge through quantile-quantile mapping: the difference between the NCEP storm tide and observed storm tide is calculated at each quantile level and these differences are added to the GCM future storm tide projections at their corresponding quantiles.

2.5. Sea Level Rise (SLR) Projection

We incorporate probabilistic, localized SLR projections from Garner et al. (2022) for the end of 21st century (2100) considering the SSP2-4.5 and SSP5-8.5 emissions scenarios. In this study, SLR probability distributions are generated for tide gauge locations across the globe by considering ice sheet components (Greenland, West Antarctic, and East Antarctic), glacier and ice cap surface mass balance, thermal expansion and oceanographic processes, water storage on land and other non-climatic factors. Sea-level changes due to thermal expansion and oceanographic processes are based on ensemble mean projections from a suite of CMIP6 GCMs. We select the nearest tide gauge to LIBH and adopt the probability distribution specified by Garner et al. (2022). The return period curves incorporate SLR by convolving the TC-induced stormtide CDF with the SLR probability density function (Lin et al., 2016; Marsooli et al., 2019).

3. Results and Discussions

3.1. Hydrodynamic Modeling

Validating both meshes for Long Island is challenging because water surface elevation observations are unavailable for Long Island and most of The Bahamas. Thus, to validate these meshes, we chose the closest U.S. coastal locations with water surface elevation observational data. Eighteen NOAA tides and current stations around Florida are picked to compare the simulations' results with the historical observation data (tidal gauge locations are shown in Appendix A). There are 23 existing NOAA tides and currents stations, but five of those stations around Florida, are too far inland, and thus are not considered for the validation.

Based on availability of the observational data and Best Track information, five major hurricanes (1—Rita 2005, 2—Irene 2011, 3—Sandy 2012, 4—Joaquin 2015, and 5—Matthew 2016) are chosen here to validate the meshes. To enforce the historical hurricanes, we use the Generalized Asymmetric Holland Model (GAHM) (Gao, 2018), which is a parametric wind and pressure model. It computes wind velocities and surface atmospheric pressures. The simulation is run for a total of 7 days on both meshes, with water surface elevations recorded from locations in the mesh corresponding to the locations of NOAA tides and currents' gauges (U.S. Geological Survey, Flood Event Viewer, N.D.). The maximum high water during these 7 days is extracted from simulations and observations. Figure 2 shows the observed peak water levels from the NOAA sensors versus the simulated peak water levels from ADCIRC on the high resolution mesh. We consider two quantities to measure the model performance: (a) root-mean-square error (RMSE), which is a measure of the magnitude of error and (b) coefficient of determination (R^2) relative to the 1:1 line, which describes how well a regression line fits a data -set. The calculated

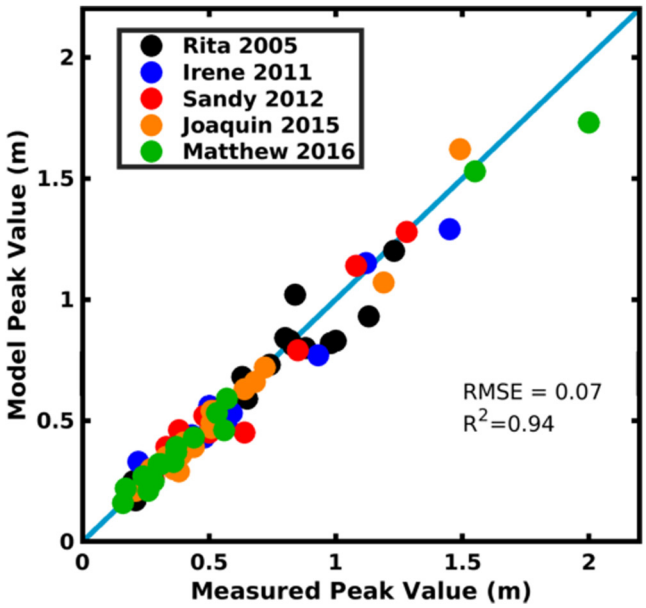

Figure 2. Comparison of observed and predicted peak water levels for the high resolution mesh. The blue solid line is 1:1 line.

RMSE value and R^2 value relative to the 1:1 line for all the hurricanes are 0.07 and 0.94, respectively. It shows that overall the model can capture the surge's peak with a reasonable agreement with the observational data.

The simulations have also performed on the coarse mesh. The maximum and the minimum errors are ±6% compared to the higher resolution. In addition, the ADCIRC model is coupled with SWAN to consider wave effects. The coupled model is run on the high resolution mesh for these five cases. The high water mark at LIBH is compared for ADCIRC and ADCIRC + SWAN models. The results from ADCIRC + SWAN are ±2% different from the ADCIRC results. However, the computational cost increases by more than two times. Therefore, run only ADCIRC. In addition, we compared our ADCIRC results with the results of Sahoo et al. (2019), who used ADCIRC + SWAN to simulate Hurricane Joaquin in 2015. The results for Long Island are in good agreement.

3.2. Event Attribution

3.2.1. Event Attribution From 1988 to 2016

We aim to pinpoint recent TCs that left coarse grained deposits in the Long Island paleohurricane record. As shown in Figure 1, three event beds in the LIBH archive dated between 1988 and 2016. Overall, 13 hurricanes passed within a radius of 100 km of LIBH between 1988 and 2016. We used the ADCIRC model with a half-kilometer mesh resolution along the coast (high-resolution mesh) to simulate all of the 13 events. We applied ADCIRC with the GAHM (Gao, 2018) for hurricanes after 2000 due to the availability of Best Track isotach data and use the symmetric Holland vortex model (Holland, 1980) for earlier storms. Note that the surge results for the GAHM model and the Holland vortex model are very close at LIBH (the difference in the peak is less than 3% at LIBH for five major hurricanes mentioned in Section 3.1). The peak of the water surface elevation at LIBH is recorded during all events and illustrated in Figure 3.

We assign the three highest LIBH surges to the three modern event beds during 1988–2016 in the paleorecord. These three events are Joaquin 2015, Irene 2011, and Lili 1996, respectively, and are consistent with the estimated ages of the samples. Among these three events, Lili 1996 generated the lowest surge, measuring 0.67 m. The fourth largest surge of 0.59 m is associated with Hurricane Frances (2004) and is also within the age estimation for the third sample. Because Frances generated a significantly smaller surge, however, we can confidently conclude that the third event bed is associated with Lili. Therefore we identify Lili's stormtide height of estimated 0.67 m to be the minimum water level a storm must generate at LIBH to leave a deposit. We refer to this water level as the deposition threshold. Note that this is a conservative choice of surge threshold. We cannot confirm whether the events that generate surges ranging between 0.59 and 0.67 m are indeed capable of producing deposition at LIBH.

3.2.2. Event Attribution From 1851 to 1987

Between 1851 and 1987 there are an additional four events that left coarse grained anomalies at LIBH. We assume the surge threshold of 0.67 m to identify these events (events 4, 5, 6, and 7 in Figure 1). Between 1851 and 1987, 53 hurricanes passed within a radius of 100 km of LIBH and therefore could have left a deposit at LIBH.

To obtain a first estimation of the storm surge from each of the 53 storms, we follow the method presented in Section 2.3. First, the central pressure and radius of maximum wind for each event are calculated. Then, we ran ADCIRC simulations for ±15 mb of the computed central pressure to account for uncertainty in estimated central pressure.

Figure 3 top panel (thick blue lines) demonstrates the range of maximum surge results obtained by varying the central pressure and radius of maximum wind. The full surge range (thick blue lines) is only shown for nine potential TCs which generated a surge above the deposition threshold established in Section 3.2.1. If the maximum surge of a storm's surge range is below this threshold, then it is represented by only its maximum surge (hollow circle).

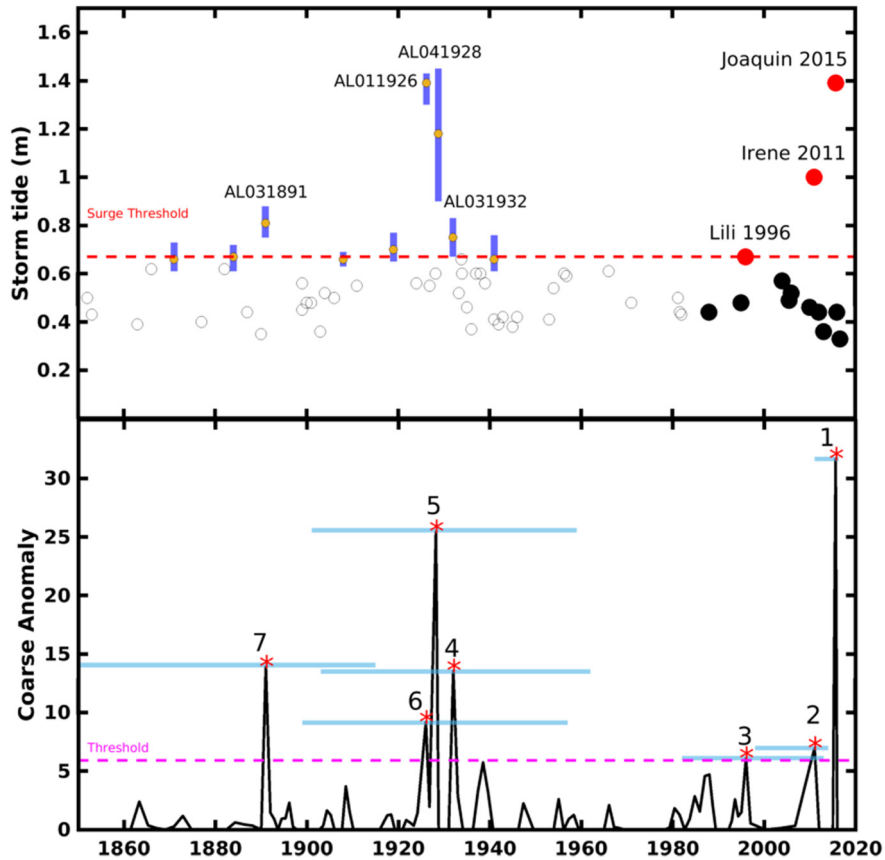

Figure 3. Top panel shows the maximum stormtide height for events from 1851 to 2016. Red dots are the stormtide height for events after 1988 that left a deposit at Long Island blue hole (LIBH). Black filled circles are the maximum stormtide for events after 1988. Empty black circles show the maximum stormtide height for events when varying the minimum central pressure. Blue lines shows the range of estimated peak stormtide when varying minimum central pressure of the storm. The yellow dots show the peak stormtide height when the pressure gradient is calculated from the empirical function (Knaff & Zehr, 2007). The dashed red line is the surge threshold of 0.67 m. The bottom panel represents the coarse anomaly data for the modern interval (1851–2016) from LIBH. The dashed magenta line is the event bed threshold of 5.90%. Starred peaks indicate identified event layers. Light blue lines represent the age uncertainty for each events.

To narrow down the nine storms to the four that most likely left deposits, we group them based on the age uncertainty of the event beds. For the oldest event (Figure 1, event 7), there are four candidate hurricanes that lead to this coarse anomaly (Figure 3). As it can be seen in Figure 3 top panel (four thick blue lines from left to right), the stormtide's height for one of these four events (AL031891) is always above the surge threshold when the minimum central pressure of hurricane is changing (±15). In addition, the stormtide's height for the median central pressure for only one event (AL031891) is above the surge threshold. As a result, we can certainly claim the first event is hurricane (AL031891), which is a Category 2 hurricane near LIBH.

For the other three events (Figure 1, events 4, 5, and 6), there are six candidates based on the age uncertainty of each event and hydrodynamic modeling results (see Figure 3 top panel, six thick blue lines from right to left). The stormtide's height for three events is always above the surge threshold when the minimum central pressure of the hurricanes varies (±15). By close inspection of the stormtide's height for the median central pressure of hurricane, we see that four events can produce stormtides' above the surge threshold. One of these events produced a stormtide height slightly less than the surge threshold (0.04 m less than the sure threshold). This event is AL021919 (the first thick blue line on the left side of AL0111926 in Figure 3). The AL021919 hurricane was a category 1 or 2 hurricane when it passed the Long Island, which is less intense than the other three events (they are category 3 and above), thus likely not leaving a deposit. Also, the stormtide's height for the median central pressure of hurricane for the AL021919 hurricane is less than other events. As a result, we can claim the AL021919 hurricane most likely had a low minimum central pressure and did not lead to sediment transport at LIBH.

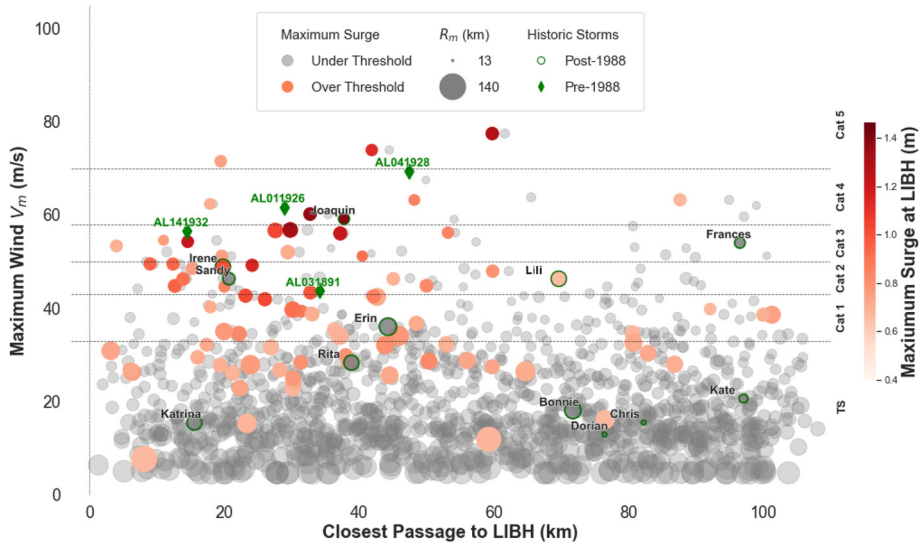

Figure 4. Storm properties of synthetic and historical storms when the storm passed closest to Long Island blue hole (LIBH). Storm's closest passage is the minimum distance between LIBH and the storm's path, regardless of which side of the site passage occurred. Historic storms are outlined in green and labeled with their names or ID if they are unnamed. Historic storms that have unknown values for radius of maximum wind (see Section 3.2.2) are marked by a diamond. Storms that generate surge above the deposition threshold of 0.67 m are colored according to their surge magnitude; storms under the deposition threshold are gray.

Amongst the nine potential historical TCs that generated surges above the deposition threshold, we attribute AL031891, AL011926, AL041928, and AL031932 to the four 1851–1988 event beds. These four storms are also the only TCs that have surge ranges entirely above the deposition threshold.

3.3. Sedimentary Record Interpretation

As seen in Section 3.2, not all storms that impact Long Island are captured in the sedimentary record. Understanding the types of storms that lead to sediment deposition at this particular site is critical to interpreting the rest of the paleorecord. Linking storm characteristics to sediment deposition in the paleorecord could offer a new avenue for estimating unknown storm properties (i.e., radius of maximum wind) for early historic storms that have corresponding event beds in the record. As the number of historic storms that left a deposit at LIBH is too limited to directly draw conclusions about the ability of different storm characteristics to cause deposition, we use the NCEP synthetic storm data from Section 2.4 in addition to historic storms to observe trends in storm characteristics.

Figure 4 illustrates key TC properties (maximum wind speed, the radius of maximum wind, and closest passage of TCs to LIBH) of the 1244 synthetic storms generated by NCEP reanalysis (see Section 2.4). All historical TCs occurring from 1851 onward are included in the figure. While the modeled maximum surge at LIBH (red shading) increases with higher intensity storms, the sediment record captures storms of a wide range of intensity and size. Among all NCEP synthetic storms (see Section 2.4), approximately 6% of storms produced a surge larger than the threshold of 0.67 m, which would result in sediment deposition at the LIBH site. Of all the storms that produced a surge larger than the threshold of 0.67 m, 3% are Category 5%, 8% are Category 4%, 13% are category 3%, 16% are category 2%, 21% are category 1%, 36% are tropical storms. Within the intensity categories, storms producing the highest surge had a radius of maximum wind on average 33.0 km larger than storms that generated surge below the 0.67 m threshold. For example, in Category 5, two storms of high intensity that did not produce a high enough surge at LIBH have an average R_{max} of 33 km which is almost half of the size other Category 5 storms (65 km on average) that generated high enough surge to theoretically cause deposition.

Even so, surge generation above the deposition threshold cannot only be isolated to storm intensity and radius of maximum wind. A storm's geographic relationship with the unique geometry and position of Long Island also influences deposition. Figure 5a shows the direction of travel and position of closest passage relative to

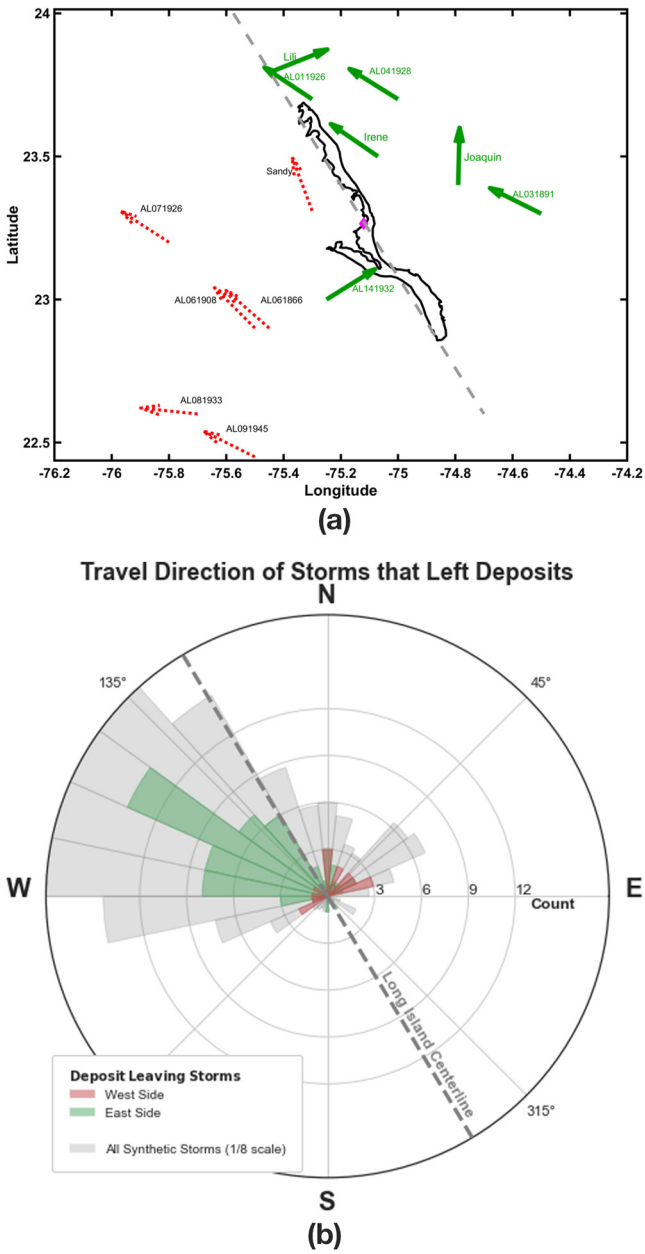

Figure 5. (a) Travel direction of historical storms direction at the point of closest passage to Long Island blue hole. The head of the arrow shows the moving direction the storm advances in the next 2 hr. Arrows are colored green if they are present in the paleorecord and red if they did not leave a deposit. The gray dashed line shows the central axis through the Long Island. (b) Radial histogram of travel directions for synthetic storms. Colors indicate which side of the island axis (gray dotted line) the storms passed on, if they left a deposit. The counts for all of the storms (gray bars) are scaled by 1/8 for figure formatting.

Long Island and LIBH for historical storms. Storms that left deposits in the paleorecord are colored solid green and six intense (above category 2 within 100 km of Long Island) storms that did not leave deposits are dotted in red. The majority of historical storms that did leave deposits passed to the east side of the central axis of Long Island (gray dashed line). West passing deposit leaving storms cross the axis orthogonally. These observations are also consistent across the synthetic storm set, as shown in Figure 5b; storms traveling parallel to the island axis must pass on the east side while west passing storms must cross the island axis at a steep angle in order to leave a deposit. Across the synthetic storms, we see that 76% of deposit leaving storms pass within 50 km of LIBH and 72% travel in a northwest direction. Conversely, high intensity historical storms moving parallel to Long Island on the west side of the axis (dotted red in Figure 5a) likely do not leave deposits at LIBH despite having high intensity and passing close to Long Island. This impact of side of passage is likely due to the complex L-shape geometry of central Long Island. This simple analysis highlights the importance of considering travel direction in addition to intensity, size, and proximity for sediment deposition at this site.

3.4. Reconstruction and Estimating Unknown Storm Properties

Figure 6 shows the K-means clusters (Duda et al., 1973) identified from the storm properties for deposit-leaving TCs introduced in Figure 4. To avoid bias from initial seed randomization, the clustering sequence is conducted 50 times, and the estimated R_{max} range is formed from the results of all iterations (Figure 6 is an example of a common clustering result). The R_{max} property is not considered when clustering as it is the property of interest.

When developing the final range of R_{max} estimations in Figure 7 for historic TCs, the synthetic storm properties' Euclidean distance from the historical reference is used to weight R_{max} distributions (i.e., the size of storms closer in passage and intensity to a historical TC will impact the estimation more).

This method of estimation is tested on modern historic TCs with known R_{max} values. The observed R_{max} values for Joaquin, Irene and Lili are all captured within the middle 90% in the range of the cluster estimate. The observed radii of maximum wind for hurricanes Joaquin, Irene, and Lili are captured in local peaks of R_{max} distribution, within 10 km of the mean R_{max} estimation, from K-means method (Figure 7a).

Additionally, estimated stormtides from the R_{max} distributions are depicted in Figure 7 bottom panel. The stormtide values for Irene and Lili are captured within the middle 10% in the range of the R_{max} cluster estimate. However, the stormtide value for Joaquin is captured within the middle 20% in the range of the R_{max} cluster estimate, likely because Hurricane Joaquin was a relatively small hurricane and moved slowly over the Island. More synthetic storms are required to train the K-means algorithm to better capture such an unusual event.

In Figure 7b, the coarse anomalies and stormtide distribution are shown from 1851 to 2016. It can be seen that for five out of seven events (hurricanes Joaquin [mean stormtide = 1.65 m, mean R_{max} = 38 km], Lili [mean stormtide = 0.58 m, mean R_{max} = 50.0 km], AL031932 [mean stormtide = 0.85 m, mean R_{max} = 47 km], AL041928 [mean stormtide = 1.1 m, mean R_{max} = 38 km], AL031891 [mean stormtide = 0.84 m, mean R_{max} = 48 km]), coarse anomaly and stormtide height distributions can be correlated. For two events (Irene [mean stormtide = 1.1 m, mean R_{max} = 37 km] and AL011926 [mean stormtide = 1.35 m, mean R_{max} = 38 km]), the coarse anomaly is much less than the simulated

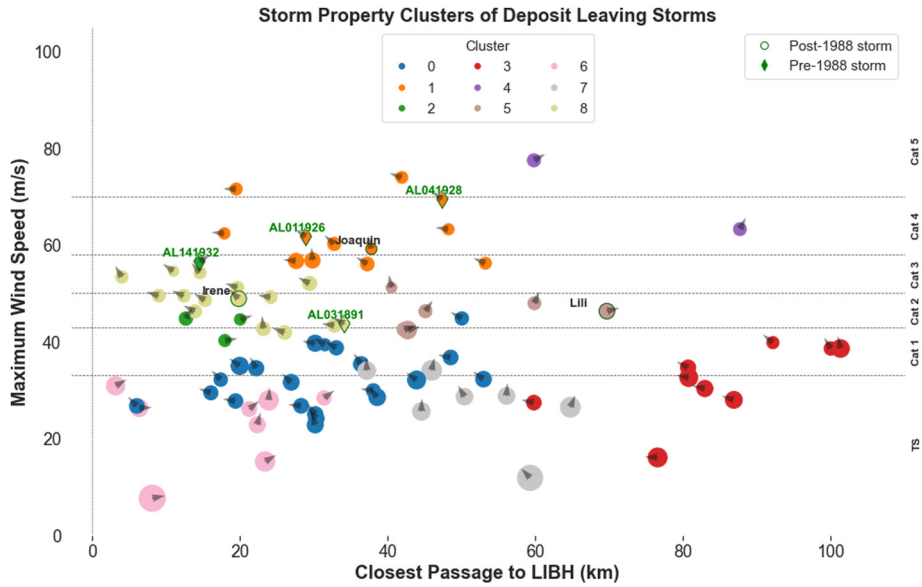

Figure 6. Clusters of shared storm characteristics (intensity, position, direction) for tropical cyclones (TCs) (synthetic and historical) generated surge over the deposition threshold. Color denotes which cluster each storm belongs to and size is the R_{max} if known. Storms without R_{max} observations are denoted by diamonds. All historic TCs are distinguished by a green outline. Directional arrows from Figure 5 are included in gray.

surge height. The most important factor causing the mismatch is the complexity of sediment transport modeling which is not considered here. Without the sediment transport modeling, we cannot establish a specific relationship between the coarse anomaly and surge height and we assume only that the surges above the identified threshold can induce deposits. Thus, the clustering analysis focuses on surge events above the threshold but do not account for the variation of the surge heights within these events. The other factors could include storm forward speed, which may influence the sediment transport process that is not considered in the K-means clustering analysis. In addition, there are uncertainties associated with hydrodynamic modeling including the half-kilometer resolution mesh on the coastline (more accurate bathymetric data is unavailable), neglecting wave effects, and using a symmetric parametric wind model. Furthermore, the limited sample of synthetic storm models introduces additional sources of uncertainty. Historical data from earlier storms also contributes to the overall uncertainty. In future work, we plan to employ a more advanced modeling approach by coupling a 3-D hydrodynamic model with sediment transport and wave models.

3.5. Surge Risk Estimation

Here, we estimate surge risk in terms of the return period of the surge height for the Long Island. To calculate the yearly probability of surge height exceedance, the theoretical distribution assumes Poisson arrival of the storms and involves a generalized Pareto distribution to model the surges over a threshold and nonparametric density estimation to model the surges smaller than the threshold (Lin, Emanuel, et al., 2010; Lin et al., 2012). Figure 8 shows the 50, 100, and 500 years spatial variation of the surge level around LIBH (calculated at each grid point) in the historical period and under the SSP2-4.5 storm climatology and SSP5-8.5 storm climatology conditions. These maps illustrate the regional distribution of storm surge risk, which varies dramatically over relatively small distances. For instance, the 500 years surge on the east side of Long Island increases from ≈1.50 m to ≈3.00 m for SSP2-4.5 and ≈ 4.75 m for SSP5-8.5. In contrast on the southwest side of Long Island the 500 years surge rises from ≈1.20 to ≈1.50 m for SSP2-4.5 and ≈ 1.80 m for SSP5-8.5, which is much less than the east side of the Island. The same trends in the surge risk maps can be observed by looking at the 100 and 50 years return periods. It demonstrates that the surge risks are controlled by bathymetry and coastline shape in addition to changes in TC climatology.

Figure 9 displays the estimated surge risk at LIBH in terms of the return period of the surge height. With only 12 historical storms passing within a 100 km radius of LIBH in the time frame of 1988–2016 (when observed

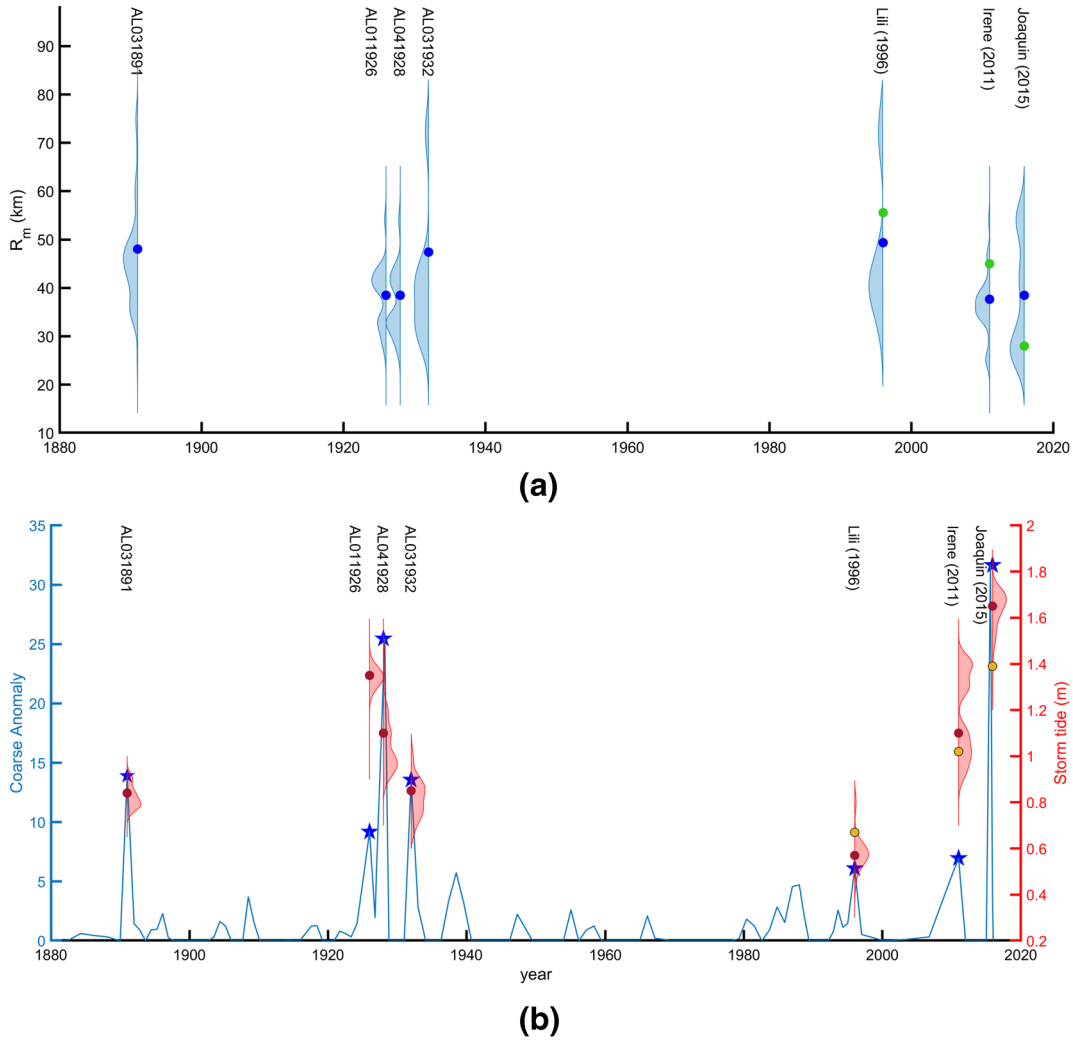

Figure 7. (a) The distribution of R_{max} by K-means method for historic tropical cyclones that occurred after and before 1988. For post-1988 storms, green markers denote for the observed R_{max} values. The blue marks show the median R_{max} value and the blue areas indicate the distribution and range of R_{max} from NCEP storms. (b) The distribution of simulated stormtide for various R_{max} by K-means method. For post-1988 storms, yellow markers show the observed stormtide values. The red marks show the stormtide values for the median R_{max} value and the red areas indicate the distribution of stormtide. The coarse anomaly values are shown with blue stars.

radius of maximum wind is available), it is not feasible to model the extreme surges using a generalized Pareto distribution. However, estimating the radius of maximum wind for hurricanes that left a deposit at LIBH between 1850 and 1988 allows us to approximate the distribution of surge height for these events (see Section 3.4). Consequently, we can use the mean of the stormtide height distributions for the four events that left deposits between 1851 and 1988 and the approximated maximum stormtide heights for the other 58 events that did not left a deposit at LIBH (see Section 3.2) to estimate the return period curve. Green circles in Figure 9 display the surge return levels based on the historic storms between 1851 and 2016. The estimated 20, 50, 100, 500, 1,000, and 5,000 years surge levels are about 0.67, 1.05, 1.30, 1.63, 1.72, and 1.84 m, respectively. The return period for the NCEP model (16 years/event) at the surge deposition threshold is close to the modern paleorecords (165 years/7 events ≈ 24 years/event). This indicates the ability of climatological-hydrodynamic modeling to capture long term risk. At more extreme levels, however, the NCEP-simulated return period curve may underestimate the surge risk. Thus, we performed the bias correction (see Section 2.4) and include the bias corrected NCEP return period curve (red dash curve in Figure 9); the bias corrected estimation of the surge levels for the various return periods are similar to those based on the reconstructed historical records.).

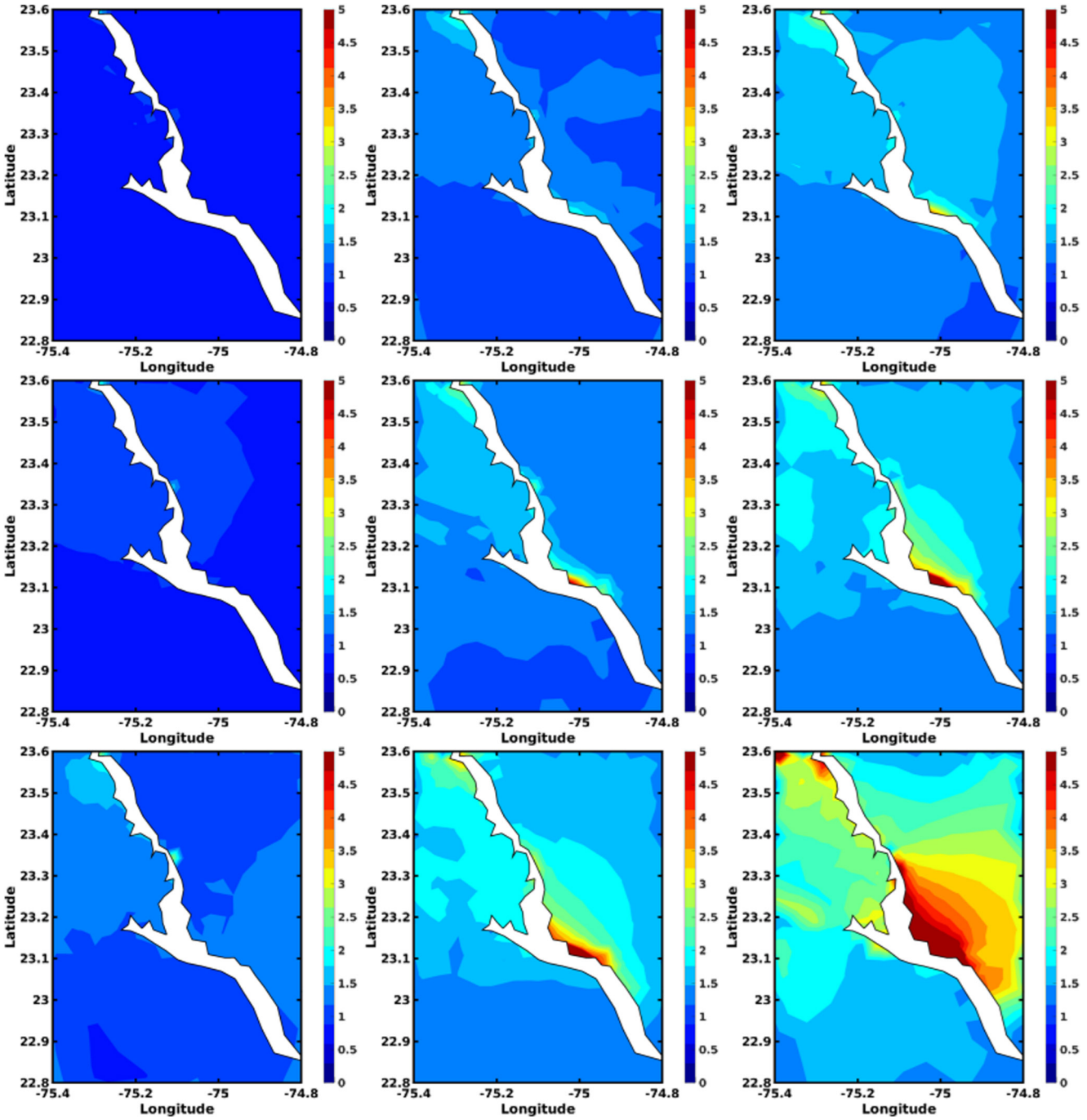

Figure 8. Surge level distribution over Long Island blue hole for 50 (first row), 100 (second row), and 500 (third row) years return period for three scenarios 1—the historical period based on NCEP reanalysis data (referred to as NCEP) (first column). 2—SSP4.5 (second column). 3—SSP8.5 (third column). Colorbars are set to cut off at 5 m for clarity of figures.

Figure 9 also includes the return period curves (bias-corrected, solid blue and black curves) for future storm climatology under carbon emission scenarios (SSP2-4.5 and SSP5-8.5). Results indicate that the flood level for a given return period substantially increases by the end of the 21st century. For instance, the 100-year surge level for SSP2-4.5 and SSP5-8.5 is 2.01 and 2.30 m, which shows a tremendous increase in risk. The very likely estimates (90% statistical confidence interval) of flood levels for a long return period cover a wide range, implying considerable statistical uncertainty in such extreme events. The uncertainties are smaller for flood levels with a higher probability of occurrence.

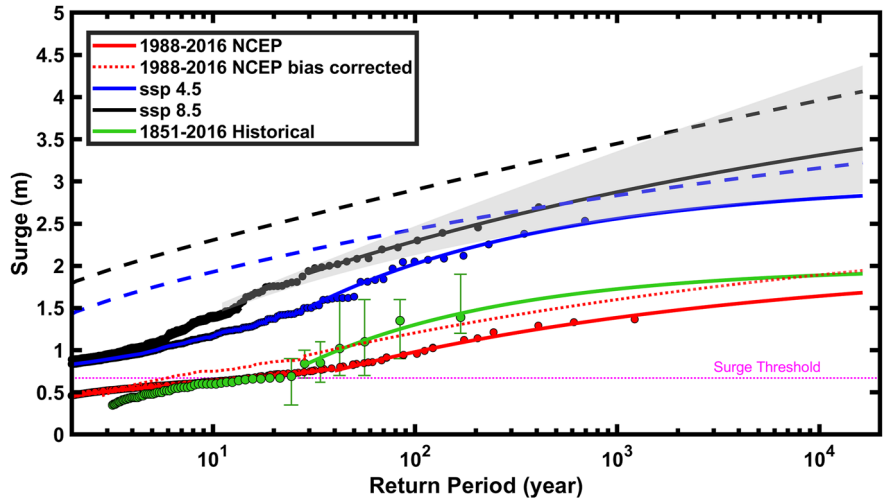

Figure 9. Estimated surge level as functions of return period. Solid lines show the best fit with the surge over threshold methods. Dashed lines are bias-corrected projection under sea level rise. The red dot dashed line is NCEP fit with bias correction using historical data 1851–2015. The shaded area show the 90% statistical confidence interval for SSP5-8.5 projection. The 90% statistical confidence interval for other curves are similar to this one, but it is not shown to avoid confusion in the figure. Green circles denote return period of surge for events between 1851 and 2015. Green bars represent the range of surge levels from Figure 7b.

Furthermore, in Figure 9, the dashed blue line represents the surge return levels considering the SSP2-4.5 storm climatology plus the projected SLR and the dashed black line denotes the surge return levels considering the SSP5-8.5 storm climatology including the effects of the projected SLR. Under the effects of SLR, the 100-year and 500-year surge levels increase from 2.01 and 2.43 m to 2.42 and 2.68 m for the SSP2-4.5 emission scenario and from 2.29 and 2.71 m to 2.92 and 3.28 m for SSP5-8.5 emission scenario, which illustrates the tremendous increase ofcoastal flood risk at the end of 21st century for this region. In other words, the 100-year flood level would occur annually for SSP2-4.5 and SSP5-8.5. The 5,000-year flood level would become a 2-year event for SSP5-8.5 and a 6-year event for SSP2-4.5, which shows a tremendous shift in the flood risk of this area. The return period of a Hurricane Joaquin level event (stormtide of 1.39 m) is expected to decrease from 145 to 23 years and 11 years under SSP2-4.5 and SSP5-8.5 storm climatology conditions, respectively. This will further reduce to 2 years and 1 year with SLR projections, illustrating how this island could become highly susceptible to large surges capable of completely inundating the area under future SLR and storm climatology change.

4. Conclusions

This work develops a methodology to interpret and leverage paleohurricane records from a site on Long Island in The Bahamas to improve long term hazard and risk estimations. The historical TC (TC) data from 1988 to 2016 at LIBH is insufficient for estimating the surge risk. To address this limitation, we leverage historical event attribution in paleorecords, coupled with synthetic storm modeling, to approximate storm parameters that are often missing in observations, such as the radius of maximum wind for storms dating 1851–1988. Then, we reconstructed surge records over 1851–2016 to verify and bias-correct the results of the climatological-hydrodynamic modeling. Finally, we assess and quantify the surge risk at the end of the 21st century by considering two carbon emission scenarios (SSP2-4.5 and SSP5-8.5), due to storm climatology and SLR.

The sediment cores from LIBH capture seven event beds during the observational record (1851–2016). A previous study (E. Wallace et al., 2019) used the SLOSH storm surge model, which does not consider the effect of tidal flows (just add the mean high tide to the initial mean sea level), to identify a few possible TCs that correspond to each paleorecord event bed. Here, using a state-of-the-art hydrodynamic model (ADCIRC), which uses higher resolution bathymetric data and considers tidal effects, we improve interpretation of the paleorecord by identifying these seven event beds specifically.

We develop a representative database of synthetic TCs with 11 times more data than available in the historical record alone. With an extended TC set, we identify trends in TC characteristics that would cause high enough

storm surge to cause deposition at LIBH. Although high intensity storms generate the most extreme surges, large surges can be produced from a wide range of storm intensity. Medium-intensity storms (categories 1–3) account for over half of storms that can leave deposits at LIBH, outnumbering deposits from intense storms (categories 4–5, 9% of depositing storms). Low and medium-intensity storms tend to have larger inner wind fields, which can create higher and more extensive surges than the more compact wind fields of higher intensity storms. A storm's orientation and coastline geometry can significantly determine whether a storm leaves a deposit. We show that six historically intense storms that passed within a radius of 100 km to LIBH did not leave deposits at this site due to the direction of passage relative to LIBH. More work is required to understand how hydrodynamics and sediment transport interact to affect deposition.

By clustering synthetic and historical storms based on these shared characteristics, we estimate the probability distribution of R_{max} for storms prior to 1988. Observed R_{max} values for Hurricanes Joaquin, Irene and Lili are all captured within the middle 90% range of the cluster estimation. We use this distribution of R_{max} values to generate informed probability distribution of stormtide for historical storms at LIBH.

With reconstructed historical stormtide records, we can evaluate and bias correct long term stormtide risk estimated by climatology-hydrodynamic modeling. The 100-year and 500-year events are then calculated to be about 1.24 and 1.46 m, respectively. The effects of SLR and TC climatology change have not been considered for most of the current flood risk mapping in this area. Considering both SLR and TC climatology change, a 100-year, 500-year, and "worst case" event are estimated to be about 2.02, 2.44, and 2.66 m for the SSP2-4.5 scenario and 2.30, 2.72, and 2.65 m for the SSP5-8.5 scenario by the end of the 21st century. An extreme event such as Joaquin in 2015 is a 150 years event under the current climate. However, considering TC climatology under the two emission scenarios, it becomes a 11-year and 10-year event and evolves to a yearly event under SLR. More frequent and more intense extreme events can change the morphology and ecosystem of the area at the end of the 21st century. We recommend that future flood mapping and flood mitigation planning in this area account for the effects of SLR and TC climatology change.

This study is the first step to reconstruct and integrate the paleoTC information in surge risk assessment. Without the assistant of complex sediment transport modeling, we assumed that the surge height above certain threshold (identified based on recent observations) can lead to coarse anomaly at LIBH, leading to uncertainties in the paleorecord reconstruction (i.e., the estimated surge heights do not match with the coarse anomalies for two out of seven events). Future analysis may improve through coupling a sediment transport model with a 3-D hydrodynamic and wave model. Nevertheless, we demonstrate the important contribution of reconstructing storm characteristics and leveraging paleorecords to improve surge risk estimation under current and future climates. The findings have important implications for surge risk assessment, providing valuable insights to enhance adaptation and mitigation investments in the study area. Moreover, the methodology employed in this study and future improvement regarding sediment transport modeling can be generally applied to other locations, offering a framework for improved interpretation of paleorecords and more accurate estimation of long-term TC risk.

Appendix A: Measurement Locations

Table A1

Table A1
Locations and Identifiers NOAA Tides and Currents Stations

Station ID	Name	Station ID	Name
8729210	Panama City Beach	8725110	Naples
8728690	Apalachicola	8724580	Key West
8727520	Cedar Key	8723970	Vaca Key
8726724	Clearwater Beach	8723214	Virginia Key, Biscayne Bay
8726520	St. Petersburg, Tampa Bay	8722956	South Port Everglades
8726607	Old Port Tampa	8722670	Lake Worth Pier, Atlantic Ocean

Table A1
Continued

Station ID	Name	Station ID	Name
8726674	East Bay	8721604	Trident Pier
8726384	Port Manatee	8720218	Mayport (Bar Pilots Dock)
8725520	Fort Myers	8720030	Fernandina Beach

Data Availability Statement

The paleorecord data presented by E. Wallace et al. (2021) are available on the websites of the National Climatic Data Center at https://www.ncdc.noaa.gov/paleo/study/32134 and the WHOI Coastal Systems Group at https://web.whoi.edu/coastal-group/data/. The best track information of historical TCs are presented by Knapp et al. (2010) and can be freely downloaded from https://ftp.nhc.noaa.gov/. The downscaled TC track information can be freely accessed online within the NSF DesignSafe-CI. This data set is created based on K. Emanuel et al. (2006).

Acknowledgments
This work was supported by the National Science Foundation (NSF), USA, via grants, ICER-1854993 and 2103754 (as part of the Megalopolitan Coastal Transformation Hub). Additionally, NSF awards 1903616 and 1854980 provided further support. Their support is gratefully acknowledged. K. Emanuel was funded by the MIT Climate Grand Challenge on Weather and Climate Extremes. This research received support by the generousity of Eric and Wendy Schmidt by recommendation of Schmidt Futures as part of its Virtual Earth System Research Institute (VESRI).

References

Babatunde, G., Emmanuel, A. A., Oluwaseun, O. R., Bunmi, O. B., & Precious, A. E. (2019). Impact of climatic change on agricultural product yield using k-means and multiple linear regressions. *Int. J. Educ. Manag. Eng.(IJEME)*, *9*(3), 16–26. https://doi.org/10.5815/ijeme.2019.03.02

Begmohammadi, A., Wirasaet, D., Poisson, A., Woodruff, J. L., Dietrich, J. C., Bolster, D., & Kennedy, A. B. (2022). Numerical extensions to incorporate subgrid corrections in an established storm surge model. *Coastal Engineering Journal*, *65*(2), 1–23. https://doi.org/10.1080/21664250.2022.2159290

Blaauw, M., & Christen, J. A. (2011). Flexible paleoclimate age-depth models using an autoregressive gamma process. *Bayesian Analysis*, *6*(3), 457–474. https://doi.org/10.1214/11-BA618

Blumenstock, D. I. (1958). Typhoon effects at Jaluit atoll in the Marshall Islands. *Nature*, *182*(4645), 1267–1269. https://doi.org/10.1038/1821267a0

Boldt, K. V., Lane, P., Woodruff, J. D., & Donnelly, J. P. (2010). Calibrating a sedimentary record of overwash from southeastern new England using modeled historic hurricane surges. *Marine Geology*, *275*(1–4), 127–139. https://doi.org/10.1016/j.margeo.2010.05.002

Brandon, C. M., Woodruff, J. D., Lane, D. P., & Donnelly, J. P. (2013). Tropical cyclone wind speed constraints from resultant storm surge deposition: A 2500 year reconstruction of hurricane activity from St. Marks, FL. *Geochemistry, Geophysics, Geosystems*, *14*(8), 2993–3008. https://doi.org/10.1002/ggge.20217

Brown, A. L., Reinhardt, E. G., van Hengstum, P. J., & Pilarczyk, J. E. (2014). A coastal Yucatan sinkhole records intense hurricane events. *Journal of Coastal Research*, *30*(2), 418–428. https://doi.org/10.2112/JCOASTRES-D-13-00069.1

Cannon, A. J., Sobie, S. R., & Murdock, T. Q. (2015). Bias correction of GCM precipitation by quantile mapping: How well do methods preserve changes in quantiles and extremes? *Journal of Climate*, *28*(17), 6938–6959. https://doi.org/10.1175/JCLI-D-14-00754.1

Carvalho, M., Melo-Gonçalves, P., Teixeira, J., & Rocha, A. (2016). Regionalization of Europe based on a k-means cluster analysis of the climate change of temperatures and precipitation. *Physics and Chemistry of the Earth, Parts A/B/C*, *94*, 22–28. https://doi.org/10.1016/j.pce.2016.05.001

Davis, R. A., Knowles, S. C., & Bland, M. J. (1989). Role of hurricanes in the Holocene stratigraphy of estuaries; examples from the Gulf Coast of Florida. *Journal of Sedimentary Research*, *59*(6), 1052–1061. https://doi.org/10.1306/212F90ED-2B24-11D7-8648000102C1865D

Davlasheridze, M., Atoba, K. O., Brody, S., Highfield, W., Merrell, W., Ebersole, B., et al. (2019). Economic impacts of storm surge and the cost-benefit analysis of a coastal spine as the surge mitigation strategy in Houston-Galveston area in the USA. *Mitigation and Adaptation Strategies for Global Change*, *24*(3), 329–354. https://doi.org/10.1007/s11027-018-9814-z

Deb, M., & Ferreira, C. M. (2018). Simulation of cyclone-induced storm surges in the low-lying delta of Bangladesh using coupled hydrodynamic and wave model (swan+ adcirc). *Journal of Flood Risk Management*, *11*(S2), S750–S765. https://doi.org/10.1111/jfr3.12254

Dietrich, J., Zijlema, M., Westerink, J., Holthuijsen, L., Dawson, C., Luettich, R., Jr., et al. (2011). Modeling hurricane waves and storm surge using integrally-coupled, scalable computations. *Coastal Engineering*, *58*(1), 45–65. https://doi.org/10.1016/j.coastaleng.2010.08.001

Dill, R. (1970). The blue hole, a structurally significant sink hole in an atoll off British Honduras. *Boletin Informativo - Asociacion Venezolana de Geologia, Mineria y Petroleo*, *13*(10), 328. Retrieved from https://eurekamag.com/research/020/228/020228278.php

Donnelly, J. P., Hawkes, A. D., Lane, P., MacDonald, D., Shuman, B. N., Toomey, M. R., et al. (2015). Climate forcing of unprecedented intense-hurricane activity in the last 2000 years. *Earth's Future*, *3*(2), 49–65. https://doi.org/10.1002/2014EF000274

Donnelly, J. P., Roll, S., Wengren, M., Butler, J., Lederer, R., & Webb, T., III. (2001). Sedimentary evidence of intense hurricane strikes from New Jersey. *Geology*, *29*(7), 615–618. https://doi.org/10.1130/0091-7613(2001)029<0615:SEOIHS>2.0.CO;2

Donnelly, J. P., & Woodruff, J. D. (2007). Intense hurricane activity over the past 5,000 years controlled by El Niño and the west African monsoon. *Nature*, *447*(7143), 465–468. https://doi.org/10.1038/nature05834

Duda, R. O., Hart, P. E., & Stork, D. G. (1973). *Pattern classification and scene analysis* (Vol. 3). Wiley New York. Retrieved from https://www.svms.org/classification/DuHS95.pdf

Egbert, G. D., & Erofeeva, S. Y. (2002). Efficient inverse modeling of Barotropic ocean tides. *Journal of Atmospheric and Oceanic Technology*, *19*(2), 183–204. https://doi.org/10.1175/1520-0426(2002)019<0183:EIMOBO>2.0.CO;2

Emanuel, K., DesAutels, C., Holloway, C., & Korty, R. (2004). Environmental control of tropical cyclone intensity. *Journal of the Atmospheric Sciences*, *61*(7), 843–858. https://doi.org/10.1175/1520-0469(2004)061<0843:ECOTCI>2.0.CO;2

Emanuel, K., Ravela, S., Vivant, E., & Risi, C. (2006). A statistical deterministic approach to hurricane risk assessment. *Bulletin of the American Meteorological Society*, *87*(3), 299–314. https://doi.org/10.1175/BAMS-87-3-299

Emanuel, K., & Rotunno, R. (2011). Self-stratification of tropical cyclone outflow. part i: Implications for storm structure. *Journal of the Atmospheric Sciences*, *68*(10), 2236–2249. https://doi.org/10.1175/JAS-D-10-05024.1

Emanuel, K. A. (2013). Downscaling CMIP5 climate models shows increased tropical cyclone activity over the 21st century. *Proceedings of the National Academy of Sciences of the United States of America*, *110*(30), 12219–12224. https://doi.org/10.1073/pnas.1301293110

(FEMA), F. E. M. A. (2012). Multi-hazard loss estimation methodology HAZUS–MH 2.1 advanced engineering building module (AEBM) technical and user's manual. Retrieved from https://www.fema.gov/sites/default/files/2020-09/fema_hazus_advanced-engineering-building-module_user-manual.pdf

Gao, J. (2018). *On the surface wind stress for storm surge modeling* (Doctoral dissertation). The University of North Carolina at Chapel Hill. Retrieved from https://www.proquest.com/dissertations-theses/on-surface-wind-stress-storm-surge-modeling/docview/2169392820/se-2

Garner, G., Hermans, T., Kopp, R., Slangen, A., Edwards, T., Levermann, A., et al. (2022). IPCC AR6 WGI sea level projections. https://doi.org/10.26050/WDCC/AR6.IPCC-DDC_AR6_Sup_SLPr

Gischler, E., Shinn, E. A., Oschmann, W., Fiebig, J., & Buster, N. A. (2008). A 1500-year Holocene Caribbean climate archive from the blue hole, lighthouse reef, Belize. *Journal of Coastal Research*, *24*(6), 1495–1505. https://doi.org/10.2112/07-0891.1

Gori, A., Lin, N., Schenkel, B., & Chavas, D. (2023). North Atlantic tropical cyclone size and storm surge reconstructions from 1950-present. *Journal of Geophysical Research: Atmospheres*, *128*(5), e2022JD037312. https://doi.org/10.1029/2022JD037312

Gori, A., Lin, N., Xi, D., & Emanuel, K. (2022). Tropical cyclone climatology change greatly exacerbates us extreme rainfall–surge hazard. *Nature Climate Change*, *12*(2), 171–178. https://doi.org/10.1038/s41558-021-01272-7

Holland, G. J. (1980). *An analytic model of the wind and pressure profiles in hurricanes*. National Emergency Training Center. Retrieved from http://danida.vnu.edu.vn/cpis/files/Refs/TCs/0-An%20Analytic%20Model%20of%20the%20Wind%20and%20Pressure%20Profiles%20in%20Hurricanes%20Holland(1980).pdf

Holland, G. J. (1982). Tropical cyclone motion: Environmental interaction plus a beta effect. Retrieved from https://apps.dtic.mil/sti/pdfs/ADA131808.pdf

Hope, M. E., Westerink, J. J., Kennedy, A. B., Kerr, P., Dietrich, J. C., Dawson, C., et al. (2013). Hindcast and validation of hurricane Ike (2008) waves, forerunner, and storm surge. *Journal of Geophysical Research: Oceans*, *118*(9), 4424–4460. https://doi.org/10.1002/jgrc.20314

Jelesnianski, C. P. (1992). *Slosh: Sea, lake, and overland surges from hurricanes* (Vol. 48). US Department of Commerce, National Oceanic and Atmospheric Administration.

Kalnay, E., Kanamitsu, M., Kistler, R., Collins, W., Deaven, D., Gandin, L., et al. (1996). The NCEP/NCAR 40-year reanalysis project. In *Renewable energy* (Vol. 77, pp. 437–471). Retrieved from https://www.taylorfrancis.com/chapters/edit/10.4324/9781315793245-16/ncep-ncar-40-year-reanalysis-project-kalnay-kanamitsu-kistler-collins-deaven-gandin-iredell-saha-white-woollen-zhu-chelliah-ebisuzaki-higgins-janowiak-mo-ropelewski-wang-leetmaa-reynolds-roy-jenne-dennis-joseph

Kennedy, A. B., Wirasaet, D., Begmohammadi, A., Sherman, T., Bolster, D., & Dietrich, J. (2019). Subgrid theory for storm surge modeling. *Ocean Modelling*, *144*, 101491. https://doi.org/10.1016/j.ocemod.2019.101491

Knaff, J. A., & Zehr, R. M. (2007). Reexamination of tropical cyclone wind–pressure relationships. *Weather and Forecasting*, *22*(1), 71–88. https://doi.org/10.1175/WAF965.1

Knapp, K. R., Kruk, M. C., Levinson, D. H., Diamond, H. J., & Neumann, C. J. (2010). The international best track archive for climate stewardship (IBTRACS) unifying tropical cyclone data [Dataset]. Bulletin of the American Meteorological Society, *91*(3), 363–376. https://doi.org/10.1175/2009BAMS2755.1

Knutson, T., Camargo, S. J., Chan, J. C., Emanuel, K., Ho, C.-H., Kossin, J., et al. (2020). Tropical cyclones and climate change assessment: Part ii: Projected response to anthropogenic warming. *Bulletin of the American Meteorological Society*, *101*(3), E303–E322. https://doi.org/10.1175/BAMS-D-18-0194.1

Lane, P., Donnelly, J. P., Woodruff, J. D., & Hawkes, A. D. (2011). A decadally-resolved paleohurricane record archived in the late Holocene sediments of a Florida sinkhole. *Marine Geology*, *287*(1–4), 14–30. https://doi.org/10.1016/j.margeo.2011.07.001

Lin, N., & Chavas, D. (2012). On hurricane parametric wind and applications in storm surge modeling. *Journal of Geophysical Research*, *117*(D9), D09120. https://doi.org/10.1029/2011JD017126

Lin, N., Emanuel, K., Oppenheimer, M., & Vanmarcke, E. (2012). Physically based assessment of hurricane surge threat under climate change. *Nature Climate Change*, *2*(6), 462–467. https://doi.org/10.1038/nclimate1389

Lin, N., Emanuel, K. A., Smith, J. A., & Vanmarcke, E. (2010). Risk assessment of hurricane storm surge for New York City. *Journal of Geophysical Research*, *115*(D18), D18121. https://doi.org/10.1029/2009JD013630

Lin, N., Kopp, R. E., Horton, B. P., & Donnelly, J. P. (2016). Hurricane Sandy's flood frequency increasing from year 1800 to 2100. *Proceedings of the National Academy of Sciences of the United States of America*, *113*(43), 12071–12075. https://doi.org/10.1073/pnas.1604386113

Lin, N., Lane, P., Emanuel, K. A., Sullivan, R. M., & Donnelly, J. P. (2014). Heightened hurricane surge risk in northwest Florida revealed from climatological-hydrodynamic modeling and paleorecord reconstruction. *Journal of Geophysical Research: Atmospheres*, *119*(14), 8606–8623. https://doi.org/10.1002/2014JD021584

Lin, N., Smith, J. A., Villarini, G., Marchok, T. P., & Baeck, M. L. (2010). Modeling extreme rainfall, winds, and surge from hurricane Isabel (2003). *Weather and Forecasting*, *25*(5), 1342–1361. https://doi.org/10.1175/2010WAF2222349.1

Liu, K.-B., & Fearn, M. L. (1993). Lake-sediment record of late Holocene hurricane activities from coastal Alabama. *Geology*, *21*(9), 793–796. https://doi.org/10.1130/0091-7613(1993)021<0793:LSROLH>2.3.CO;2

Liu, K.-B., & Fearn, M. L. (2000). Reconstruction of prehistoric landfall frequencies of catastrophic hurricanes in northwestern Florida from lake sediment records. *Quaternary Research*, *54*(2), 238–245. https://doi.org/10.1006/qres.2000.2166

Luettich, R. A., Westerink, J. J., & Scheffner, N. W. (1992). *Adcirc: An advanced three-dimensional circulation model for shelves, coasts, and estuaries. Report 1, theory and methodology of ADCIRC-2DD1 and ADCIRC-3DL*. Coastal Engineering Research Center (US). Retrieved from http://hdl.handle.net/11681/4618

Maloney, E. D., & Hartmann, D. L. (2000). Modulation of hurricane activity in the gulf of Mexico by the Madden-Julian oscillation. *Science*, *287*(5460), 2002–2004. https://doi.org/10.1126/science.287.5460.2002

Marsooli, R., & Lin, N. (2018). Numerical modeling of historical storm tides and waves and their interactions along the us east and gulf coasts. *Journal of Geophysical Research: Oceans*, *123*(5), 3844–3874. https://doi.org/10.1029/2017JC013434

Marsooli, R., Lin, N., Emanuel, K., & Feng, K. (2019). Climate change exacerbates hurricane flood hazards along US Atlantic and gulf coasts in spatially varying patterns. *Nature Communications*, *10*(1), 1–9. https://doi.org/10.1038/s41467-019-11755-z

Maxwell, J. T., Bregy, J. C., Robeson, S. M., Knapp, P. A., Soulé, P. T., & Trouet, V. (2021). Recent increases in tropical cyclone precipitation extremes over the US east coast. *Proceedings of the National Academy of Sciences of the United States of America*, *118*(41), e2105636118. https://doi.org/10.1073/pnas.2105636118

McCloskey, T., & Keller, G. (2009). 5000 year sedimentary record of hurricane strikes on the central coast of Belize. *Quaternary International*, *195*(1–2), 53–68. https://doi.org/10.1016/j.quaint.2008.03.003

McKee, E. D. (1959). Storm sediments on a pacific atoll. *Journal of Sedimentary Research*, *29*(3), 354–364. https://doi.org/10.1306/74D7092A-2B21-11D7-8648000102C1865D

Pringle, W. J., Wirasaet, D., Roberts, K. J., & Westerink, J. J. (2021). Global storm tide modeling with ADCIRC v55: Unstructured mesh design and performance. *Geoscientific Model Development*, *14*(2), 1125–1145. https://doi.org/10.5194/gmd-14-1125-2021

Robbie, B. (2016). *Tropical cyclone report, hurricane Joaquin (al112015) 28 September – 7 October 2015* (pp. 1–36). National Hurricane Center. https://doi.org/10.1175/JAS-D-17-0137.1

Roberts, K. J., Pringle, W. J., & Westerink, J. J. (2019). OceanMesh2d 1.0: Matlab-based software for two-dimensional unstructured mesh generation in coastal ocean modeling. *Geoscientific Model Development*, *12*(5), 1847–1868. https://doi.org/10.5194/gmd-12-1847-2019

Roelvink, J., & Van Banning, G. (1995). Design and development of DELFT3D and application to coastal morphodynamics. *Oceanographic Literature Review*, *11*(42), 925.

Sahoo, B., Jose, F., & Bhaskaran, P. K. (2019). Hydrodynamic response of Bahamas archipelago to storm surge and hurricane generated waves–a case study for hurricane Joaquin. *Ocean Engineering*, *184*, 227–238. https://doi.org/10.1016/j.oceaneng.2019.05.026

Scheffner, N. W., Borgman, L. E., & Mark, D. J. (1996). Empirical simulation technique based storm surge frequency analyses. *Journal of Waterway, Port, Coastal, and Ocean Engineering*, *122*(2), 93–101. https://doi.org/10.1061/(ASCE)0733-950X(1996)122:2(93)

Schmitt, D., Gischler, E., Anselmetti, F. S., & Vogel, H. (2020). Caribbean cyclone activity: An annually-resolved common era record. *Scientific Reports*, *10*(1), 11780. https://doi.org/10.1038/s41598-020-68633-8

Shinn, E. A., Reich, C. D., Locker, S. D., & Hine, A. C. (1996). A giant sediment trap in the Florida keys. *Journal of Coastal Research*, 953–959. Retrieved from https://www.jstor.org/stable/4298545

Tan, F., Zhang, Y., Cao, L., Xu, H., Shi, Q., Zhang, X., et al. (2023). Meridional response of western north pacific paleocyclone activity to tropical atmospheric circulation variability over the past millennium. *Palaeogeography, Palaeoclimatology, Palaeoecology*, *610*, 111331. https://doi.org/10.1016/j.palaeo.2022.111331

Tao, S., Liu, K.-B., Yu, K., Shi, Q., Yan, H., Zhang, H., et al. (2021). Poleward shift in tropical cyclone tracks in the northwest pacific during warm periods: Past and future. *Paleoceanography and Paleoclimatology*, *36*(12), e2021PA004367. https://doi.org/10.1029/2021PA004367

Tokdar, S. T., & Kass, R. E. (2010). Importance sampling: A review. *Wiley Interdisciplinary Reviews: Computational Statistics*, *2*(1), 54–60. https://doi.org/10.1002/wics.56

Toro, G. R., Resio, D. T., Divoky, D., Niedoroda, A. W., & Reed, C. (2010). Efficient joint-probability methods for hurricane surge frequency analysis. *Ocean Engineering*, *37*(1), 125–134. https://doi.org/10.1016/j.oceaneng.2009.09.004

Tozer, B., Sandwell, D. T., Smith, W. H., Olson, C., Beale, J., & Wessel, P. (2019). Global bathymetry and topography at 15 arc sec: Srtm15+. *Earth and Space Science*, *6*(10), 1847–1864. https://doi.org/10.1029/2019EA000658

U.S. Geological Survey, Flood Event Viewer. (N.D.). Website. Retrieved from https://stn.wim.usgs.gov/FEV/

van Hengstum, P. J., Donnelly, J. P., Toomey, M. R., Albury, N. A., Lane, P., & Kakuk, B. (2014). Heightened hurricane activity on the little bahama bank from 1350 to 1650 ad. *Continental Shelf Research*, *86*, 103–115. https://doi.org/10.1016/j.csr.2013.04.032

Vickery, P., Skerlj, P., & Twisdale, L. (2000). Simulation of hurricane risk in the US using empirical track model. *Journal of Structural Engineering*, *126*(10), 1222–1237. https://doi.org/10.1061/(ASCE)0733-9445(2000)126:10(1222)

Virgil, K. (N.D.). Hurricane wiped out 836 homes. In *The tribune*. Retrieved from http://www.tribune242.com/news/2015/oct/22/hurricane-wiped-out-836-homes/?news

Wallace, E. J., Donnelly, J., van Hengstum, P., Winkler, T., McKeon, K., MacDonald, D., et al. (2021). 1,050 years of hurricane strikes on long island in the Bahamas [Dataset]. Paleoceanography and Paleoclimatology, *36*(3), e2020PA004156. https://doi.org/10.1029/2020PA004156

Wallace, E. J., Donnelly, J. P., van Hengstum, P. J., Wiman, C., Sullivan, R., Winkler, T., et al. (2019). Intense hurricane activity over the past 1500 years at south Andros Island, the Bahamas. *Paleoceanography and Paleoclimatology*, *34*(11), 1761–1783. https://doi.org/10.1029/2019PA003665

Wallace, E. J., Dee, S. G., & Emanuel, K. A. (2021). Resolving long-term variations in North Atlantic tropical cyclone activity using a pseudo proxy paleotempestology network approach. *Geophysical Research Letters*, *48*(18), 1–13. https://doi.org/10.1029/2021gl094891

Wallace, E. J., Donnelly, J. P., van Hengstum, P. J., Winkler, T. S., Dizon, C., LaBella, A., et al. (2021). Regional shifts in paleohurricane activity over the last 1500 years derived from blue hole sediments offshore of Middle Caicos Island. *Quaternary Science Reviews*, *268*, 1–18. https://doi.org/10.1016/j.quascirev.2021.107126

Winkler, T. S., van Hengstum, P. J., Donnelly, J. P., Wallace, E. J., Sullivan, R. M., MacDonald, D., & Albury, N. A. (2020). Revising evidence of hurricane strikes on Abaco island (the Bahamas) over the last 700 years. *Scientific Reports*, *10*(1), 16556. https://doi.org/10.1038/s41598-020-73132-x

Woodruff, J. D., Irish, J. L., & Camargo, S. J. (2013). Coastal flooding by tropical cyclones and sea-level rise. *Nature*, *504*(7478), 44–52. https://doi.org/10.1038/nature12855

Yang, Y., Piper, D. J., Normandeau, A., Zhou, L., Jia, J., Wang, Y. P., & Gao, S. (2022). A late Holocene shift of typhoon activity recorded by coastal sedimentary archives in eastern China. *Sedimentology*, *69*(2), 954–969. https://doi.org/10.1111/sed.12934

Yang, Y., Zhou, L., Normandeau, A., Jia, J., Yin, Q., Wang, Y. P., et al. (2020). Exploring records of typhoon variability in eastern China over the past 2000 years. *GSA Bulletin*, *132*(11–12), 2243–2252. https://doi.org/10.1130/B35600.1